

Time Since Burning and Rainfall Characteristics Impact Post-Fire Debris-Flow Initiation and Magnitude

LUKE A. MCGUIRE*

*University of Arizona, Department of Geosciences, 1040 East 4th Street, Tucson,
AZ 85721*

FRANCIS K. RENGERS

U.S. Geological Survey, 1711 Illinois Street, Golden, CO 80401

NINA OAKLEY

*Western Regional Climate Center, Desert Research Institute, 2215 Raggio Parkway,
Reno, Nevada 89512, USA*

JASON W. KEAN
DENNIS M. STALEY

U.S. Geological Survey, 1711 Illinois Street, Golden, CO 80401

HUI TANG

*Section 4.7, Earth Surface Process Modeling, German Research Center for Geosciences
(GFZ), Telegrafenberg, Building A 27, 14473 Potsdam, Germany*

MARIAN DE ORLA-BARILE

*Center for Western Weather and Water Extremes, Scripps Institute of Oceanography,
9500 Gilman Drive, La Jolla, CA 92037*

ANN M. YOUNBERG

*University of Arizona, Arizona Geological Survey, 1955 East 6th Street, Tucson,
AZ 85721*

Key Terms: *Wildfire, Threshold, Infiltration, Erosion, Geomorphology*

ABSTRACT

The extreme heat from wildfire alters soil properties and incinerates vegetation, leading to changes in infiltration capacity, ground cover, soil erodibility, and rainfall interception. These changes promote elevated rates of runoff and sediment transport that increase the likelihood of runoff-generated debris flows. Debris flows are most common in the year immediately following wildfire, but temporal changes in the likelihood and magnitude of debris flows following wildfire are not well constrained. In this study, we combine measurements of soil-hydraulic properties with vegetation survey data and numerical modeling to understand how debris-flow threats are

likely to change in steep, burned watersheds during the first 3 years of recovery. We focus on documenting recovery following the 2016 Fish Fire in the San Gabriel Mountains, California, and demonstrate how a numerical model can be used to predict temporal changes in debris-flow properties and initiation thresholds. Numerical modeling suggests that the 15-minute intensity-duration (ID) threshold for debris flows in post-fire year 1 can vary from 15 to 30 mm/hr, depending on how rainfall is temporally distributed within a storm. Simulations further demonstrate that expected debris-flow volumes would be reduced by more than a factor of three following 1 year of recovery and that the 15-minute rainfall ID threshold would increase from 15 to 30 mm/hr to greater than 60 mm/hr by post-fire year 3. These results provide constraints on debris-flow thresholds within the San Gabriel Mountains and highlight the importance of considering local rainfall characteristics when using numerical models to assess debris-flow and flood potential.

*Corresponding author email: lmcguire@email.arizona.edu

INTRODUCTION

Wildfire is a well-documented catalyst for change in hydrologic and geomorphic systems (e.g., Shakesby and Doerr, 2006). Post-wildfire reductions in infiltration capacity (Ebel and Moody, 2017) and canopy interception (Stoof et al., 2012) promote increased runoff. Increased runoff, combined with the effects of lower critical thresholds for sediment entrainment (Moody et al., 2005) and a high percentage of bare soil, leads to a substantial increase in debris-flow likelihood after a wildfire. Post-wildfire debris flows are often generated when runoff concentrates in steep channels and mobilizes large volumes of sediment in contrast to debris flows that initiate from shallow landslides (e.g., Meyer and Wells, 1997; Cannon et al., 2008; Gabet and Bookter, 2008; and Kean et al., 2011). With few exceptions (e.g., Cannon et al., 2008), previous work has focused on the threats posed by runoff-generated debris flows in the first year following disturbance by wildfire; therefore, the extent to which debris-flow hazards persist into subsequent years is not well understood.

Rainfall intensity-duration (ID) thresholds are commonly used to assess post-wildfire debris-flow potential, with debris flows often initiating once a critical rainfall intensity is exceeded (Cannon et al., 2008; Staley et al., 2013). Staley et al. (2017) recently developed an empirical model to predict debris-flow likelihood as a function of terrain attributes, soil burn severity, and rainfall intensity (averaged over 15, 30, or 60 minutes). However, it is not clear how rainfall ID thresholds change with time following wildfire because data regarding debris-flow occurrence are most common in the first post-wildfire year and because there is no clear connection between the magnitude of empirically derived rainfall ID thresholds and the hydrologic and geomorphic variables that are changing as the landscape recovers. Since overland flow is a necessary condition for runoff-generated debris flows, it is critical to understand how wildfire-driven changes to soil infiltration capacity vary with time since burning and how the magnitude of those changes translates into changes in debris-flow potential. Post-wildfire reductions in infiltration capacity are often attributed to surface soil sealing (Larsen et al., 2009), hyper-dry conditions (Moody and Ebel, 2012), or increased soil water repellency (DeBano, 2000; Shakesby and Doerr, 2006), which may persist for up to 5 years but typically decays over timescales of 1–2 years (e.g. Larsen et al., 2009). The percentage of bare soil, which is initially high following wildfire and decreases as vegetation recovers, is also likely to be a key factor in determining debris-flow potential since bare soil on hillslopes is particularly vulnerable to erosion. Hillslope erosion can account for a substantial amount of the sediment within post-

wildfire debris flows in certain cases (e.g. Smith et al., 2012; Staley et al., 2014; and Rengers et al., 2016b) and contribute to sediment bulking in the channel that increases flow depth and discharge.

In addition to a lack of data regarding how debris-flow likelihood varies with time following a fire, there is also a general need to assess the extent to which debris-flow properties can be predicted by simple metrics that summarize rainfall characteristics, such as the peak 15-minute average rainfall intensity (I_{15}). It is common practice to use rainfall intensity, averaged over a specified duration, to assess the potential for debris flows (Staley et al., 2013). Similarly, empirical models used to predict the volume of post-fire debris flows rely on simple measures of rainfall characteristics, including I_{15} (Gartner et al., 2014). Such methods have proved invaluable for rapid assessments of post-fire debris-flow hazards. There is also reason to believe that I_{15} is a particularly useful metric for predicting the initiation and magnitude of post-fire debris flows because runoff generates these flows and the magnitude of post-wildfire runoff at the watershed scale correlates well with rainfall over timescales of 10–15 minutes (Kean et al., 2011; Raymond et al., 2020). However, given the sensitivity of runoff and sediment transport to rainfall intensity, it is reasonable to assume that two rainstorms could have the same peak 15-minute rainfall intensity but still produce different debris-flow responses. Consider the extreme case where the rainfall intensity is 10 mm/hr for 5 minutes, rapidly increases to 100 mm/hr for 5 minutes, and then returns to an intensity of 10 mm/hr for 5 minutes. The runoff and debris-flow response resulting from this type of storm, which would have a peak I_{15} of 40 mm/hr, may be quite different from that of a storm where the rainfall intensity is constant at 40 mm/hr.

Rapid increases in rainfall intensity over short durations are not uncommon in nature, including in southern California, where they typically accompany rainstorms classified as narrow cold-frontal rain bands (NCFRs). NCFRs are narrow bands (often <5 km wide) of high-intensity rainfall occurring parallel to and in the proximity of a cold front (Figure 1). NCFRs have a history of triggering post-fire debris flows in the Transverse Ranges of southern California (Oakley et al., 2017, 2018). In January 2018, an NCFR impacted the burn scar of the 2018 Thomas Fire, triggering debris flows that produced widespread damage and resulted in 23 fatalities (Oakley et al., 2018; Kean et al., 2019). Here, we provide a simple example using two distinct hyetographs, one for an NCFR and one with a Gaussian distribution, to evaluate how the shape of the rainfall hyetograph (e.g., I_5/I_{15}) influences debris-flow response for the same I_{15} . To the extent that particular rainfall hyetograph characteristics can be linked to

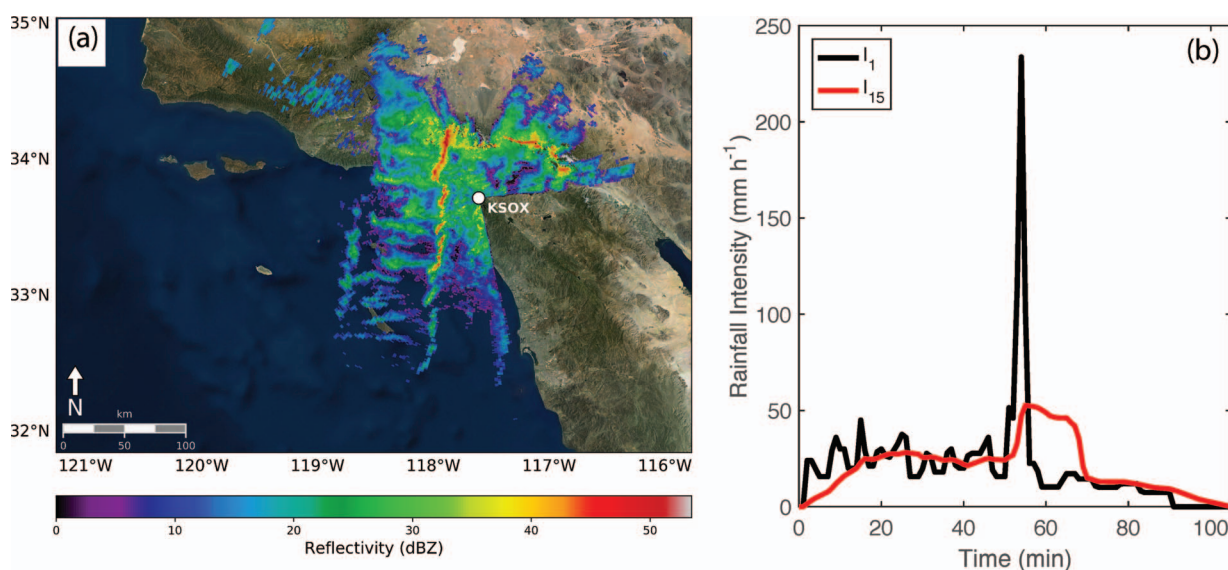


Figure 1. (a) Base reflectivity (dBZ) from the NEXRAD weather radar in Santa Ana (KSOX) at 19:32 UTC on January 2, 2006, showing a narrow cold-frontal rain band. Warmer colors indicate higher-intensity precipitation, while cooler colors indicate lighter precipitation. (b) Time series of the 1-minute and 15-minute average rainfall intensity based on measured rainfall at the Clear Creek School gauge. Time is in minutes from 18:16 UTC on January 2, 2006.

storm type (e.g., NCFR, isolated convective cells), this is a first step toward understanding the role of storm type on post-fire debris-flow initiation and magnitude. Understanding the storm types most likely to produce impactful debris flows would improve the situational awareness of weather forecasters who may be tasked with the responsibility of issuing warnings for communities downstream of burned areas.

In this study, we combine site measurements of soil-hydraulic properties and canopy/ground cover with a physically based numerical model to explore how changing site characteristics influence the initiation and magnitude of runoff-generated debris flows. The numerical model, developed by McGuire et al. (2017), represents the coupled processes of runoff, sediment transport, and debris-flow initiation. In addition to changing site characteristics, we force this model with two different rainstorms—one that is an idealized storm with a rainfall time series that has the shape of a Gaussian distribution and one that is more representative of rainfall conditions associated with an NCFR—to assess the sensitivity of results to differences in rainfall characteristics. We hypothesize that (1) the I_{15} threshold for debris-flow initiation will be sensitive to the temporal distribution of rainfall (i.e., NCFRs versus a Gaussian distribution of rainfall), (2) the I_{15} threshold will increase with time following wildfire, and (3) the typical volume of debris flows will decrease with time following wildfire. Moreover, we aim to quantify the timescale for substantial recovery of soil-hydraulic properties following wildfire and pro-

vide physical explanations for any trends observed between time since burning, debris-flow initiation thresholds, and debris-flow volume.

STUDY AREA

The study area, which we refer to as Las Lomas, is located near the headwaters of a 0.1-km² watershed that drains into the Las Lomas debris basin (Figure 2). Data from the Las Lomas study site are used to quantify changes in soil-hydraulic properties and canopy/ground cover with time following the 2016 Fish Fire. The Fish Fire, which started on June 21, 2016, burned 4,253 acres of the Angeles National Forest in the San Gabriel Mountains (SGM) near Los Angeles, California (Figure 2). The wildfire burned in rugged terrain with steep hillslopes dominated by chaparral vegetation. Soils in the SGM are generally thin (0.5–1 m), rock outcrops are common, and a highly weathered layer of saprolite is occasionally exposed on the hillslopes (Staley et al., 2014). Based on particle size analysis of hillslope sediment at the site, the soil texture is classified as sandy loam (Tang et al., 2019). Repeat measurements of soil-hydraulic properties were conducted on a roughly 40° hillslope in an area that, based on field observations and the severity indicators described by Parson et al. (2010), experienced moderate to high soil burn severity during the Fish Fire. No vegetation canopy remained, all litter and duff at the surface had been consumed by the wildfire, and soils were generally water repellent at/near

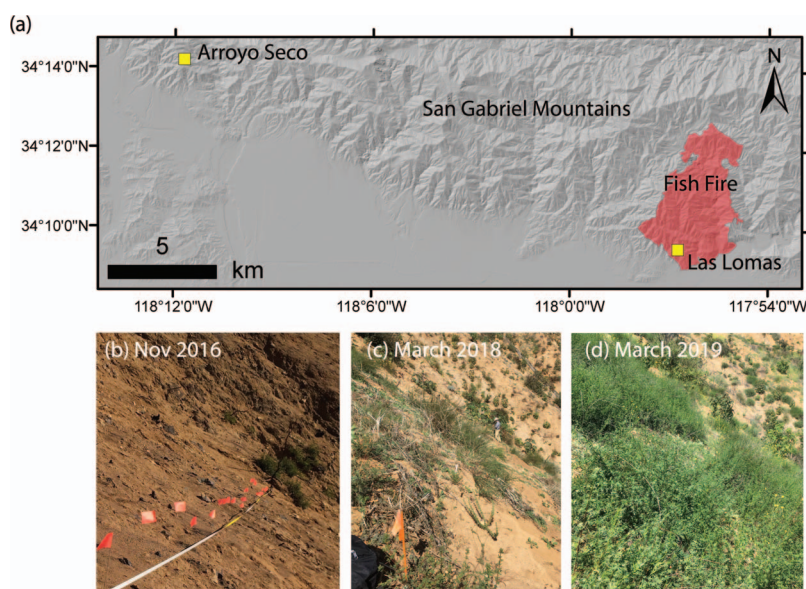


Figure 2. (a) Overview of study area. (b–d) Photos looking across the hillslope along a transect at the Las Lomas site where infiltration measurements were conducted.

the surface. A series of rainstorms between December 2016 and February 2017 incised a network of rills through the study area and produced a number of debris flows and floods at the outlet of the drainage basin (Tang et al., 2019).

METHODS

Field Measurements Following the Fish Fire

Field-saturated hydraulic conductivity (K_s) and sorptivity (S) were determined through *in situ* measurements conducted with a mini disk tension infiltrometer over a 33-month period following the wildfire. The tension infiltrometer has a disk with a radius of 2.25 cm. The suction head was set to 1 cm for all measurements. Measurements were made during site visits to the Las Lomas study area in September 2016, November 2016, January 2017, February 2017, July 2017, March 2018, and March 2019. Measurements were performed every 1 m along a 20-m transect that extended in the cross-slope direction, with the exception of those made in September 2016. When time permitted, additional measurements were made on the hillslope in the vicinity of the established transect. In September 2016, the transect had not yet been established, and measurements were made in nearby areas burned at moderate or high severity.

A total of 22, 31, 26, 37, 20, 21, and 20 infiltration measurements were made during the site visits in September 2016, November 2016, January 2017, February 2017, July 2017, March 2018, and March

2019, respectively. During each measurement, the total volume of water infiltrated is tracked as a function of time and must later be post-processed to infer field-saturated hydraulic conductivity (K_s) and sorptivity (S) (e.g., Zhang, 1997). Estimates of K_s and S were derived following the methodology of Zhang (1997). Letting I denote the total volume infiltrated at time t during the measurement, $I = C_1\sqrt{t} + C_2t$, where $C_1 = A_1S$, $C_2 = A_2K_s$, and $A_1 = 3.89$ and $A_2 = 1.04$ are empirical coefficients whose values depend on soil texture. Since I and t are known at various times throughout each measurement, we determined C_1 and C_2 using the three different curve-fitting techniques proposed by Vandervaere et al. (2000). For each mini disk measurement, this results in three estimates of S and K_s that are then averaged to obtain single values for S and K_s . The wetting front suction head (h_f), a parameter in the Green-Ampt infiltration model, can then be estimated as $h_f = S^2/2K_s\theta_s$ (Ebel and Moody, 2017), where $\theta_s = 0.4$ denotes the volumetric water content at saturation. In some instances, however, it was clear that the infiltration data did not follow the trend suggested by the equation $I = C_1\sqrt{t} + C_2t$. This could be due to error during the measurement process, such as poor contact between the mini disk and the soil surface, or could be the result of a layered system (e.g., a thin water-repellent layer on top of a more wettable soil) that is not well described by the assumed infiltration model. In these cases, we could not obtain estimates for S and K_s .

In March 2018 and March 2019, we conducted vegetation surveys on a hillslope adjacent to the

infiltration transect using the point-intercept method (e.g., Crocker and Tiver, 1948). A measuring tape was extended, and measurements were taken on 20-cm intervals along the transect (105 measurements in 2018 and 76 in 2019). We sighted directly down toward the surface with a laser pointer and recorded the first obstacle that intercepted the light. The laser hit either the vegetation canopy, bare soil, litter, or a rock. Litter was classified as any loose plant material on the soil surface. Any sediment with a diameter greater than 5 mm was classified as rock cover. If the laser hit any portion of the canopy, the maximum height of that vegetation was recorded.

Numerical Model

The numerical model represents fluid flow using the shallow-water equations, which contain additional source terms to account for changes in flow resistance as a function of sediment concentration (McGuire et al., 2016, 2017). The model is described in detail by McGuire et al. (2016, 2017) and is only briefly summarized here. Infiltration is modeled with the Green-Ampt equation, using estimates of K_s and h_f obtained from field measurements. The infiltration capacity of the soil (I_c) is given by

$$I_c = K_s \left(\frac{Z_f + h_f + h}{Z_f} \right),$$

where h denotes flow depth, $Z_f = V/(\theta_s - \theta_i)$ is the depth of the wetting front, V is the total depth of water infiltrated, and θ_i is the initial volumetric soil water content. Hydraulic roughness was represented using a depth-dependent Manning friction coefficient (Mügler et al., 2011). More specifically, the Manning coefficient varies in space and time according to

$$n = \begin{cases} n_0 \left(\frac{h}{h_c} \right)^{-0.33} & h \leq h_c, \\ n_0 & h > h_c, \end{cases}$$

where $h_c = 0.003$ m is a critical flow depth. The coefficient n_0 is calibrated.

The Hairsine-Rose model (Hairsine and Rose, 1992a, 1992b) is used to account for sediment entrainment and deposition, as described in detail by McGuire et al. (2016). In the Hairsine-Rose model, particles can be detached and entrained into the flow via raindrop impact or flow-driven detachment. The rate at which sediment is detached by raindrops is a function of flow depth, rainfall intensity, and raindrop diameter, while the rate of flow-driven sediment detachment is a function of stream power. Since the canopy and ground cover (e.g., litter) can shield the underlying soil from raindrop impact, changes in ground and canopy cover will also influence the rate of

raindrop-driven sediment detachment (e.g., McGuire et al., 2016).

Sediment being transported by the flow can also influence flow rheology. In regions of flow where the sediment concentration is below 20 percent, flow resistance is accounted for solely through the above Manning-type equation. In regions of flow where the sediment concentration is above 40 percent, we account for additional resistance associated with debris flow using a Coulomb friction approach (e.g., Iverson and Denlinger, 2001) where the effective basal normal stress is modified by pore-fluid pressure within the flow. In all simulations, the ratio of pore-fluid pressure to total basal normal stress (λ) is set to a constant value of $\lambda = 0.65$. A debris flow is identified within the model as flow with a sediment concentration above 40 percent. At intermediate sediment concentrations between 20 and 40 percent, the magnitude of the debris-flow resistance term is scaled by a multiplicative factor that ranges from 0 at a sediment concentration of 20 percent to 1 at a sediment concentration of 40 percent. Varying flow resistance terms as a function of sediment concentration enables the model to better represent the transition from water-dominated flow to debris flow.

The onset and magnitude of runoff generated by the model depends on the infiltration capacity of the soil as predicted by the Green-Ampt equation and the rainfall hyetograph. Runoff, in turn, facilitates sediment transport that leads to changes in topography and, potentially, to debris flow initiation. The model is capable of generating debris flows through two different mechanisms. First, it is possible that hydrologic conditions and sediment availability promote substantial entrainment and limited deposition of sediment. In this case, sediment concentration (c) may exceed that typically associated with debris flows in the model (e.g., $c > 40$ percent) as a result of the progressive addition of sediment to the flow column. This style of debris flow initiation is similar to the progressive bulking mechanism that has been described in past studies (e.g., Cannon et al., 2001; Gabet and Bookter, 2008). Debris flows may also initiate within the model as a result of the en masse failure of bed sediment along a failure plane (e.g., Takahashi, 1978; Kean et al., 2013). This scenario often develops in the model when there are areas of preferential deposition, such as channel reaches with relatively low slopes, that lead to the formation of a sediment dam. If the deposited sediment becomes unstable as a mass, it fails and can lead to the formation of a debris flow surge if the added sediment volume is sufficient to locally increase the sediment concentration above 40 percent. The stability of a deposited mass of sediment is determined locally using a factor of safety based on the ratio of resisting

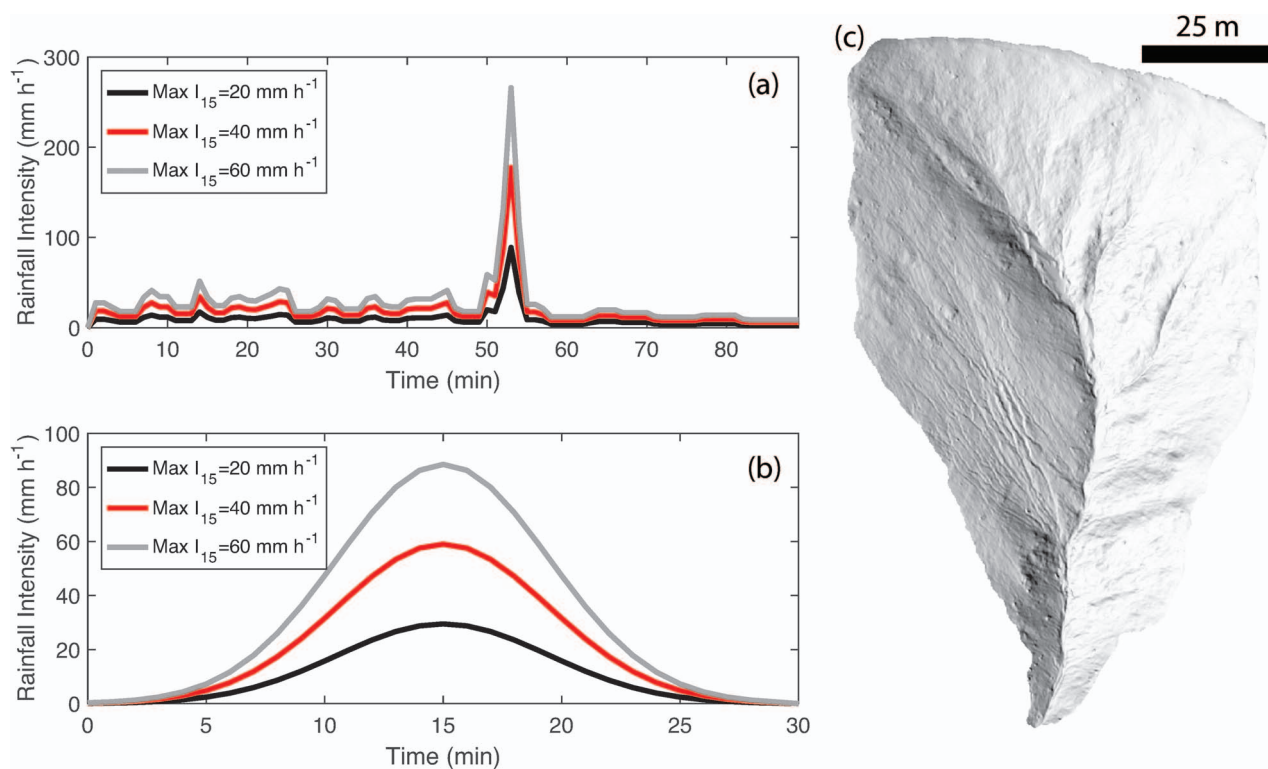


Figure 3. (a) Rainfall time series typical of narrow cold-frontal rain bands with different peak 15-minute rainfall intensities. (b) Idealized rainstorms with rainfall intensity shaped like a Gaussian function. For display purposes, only three curves are shown; however, for modeling, we used curves with peak 15-minute rainfall intensity (I_{15}) varying from 10 to 60 mm/hr in intervals of 5 mm/hr. (c) Shaded relief map of the Arroyo Seco watershed.

and driving forces acting on a column of sediment. If the driving forces are greater than the resisting forces at a particular model grid cell, then the column of sediment is determined to be unstable, and the sediment in that grid cell is instantaneously added to the above flow. A complete description of the failure criteria used in the model is given by McGuire et al. (2017).

Debris-Flow Simulations

In model simulations, we applied the vegetation and hydrologic measurements to simulate runoff, sediment transport, and debris-flow initiation within a 0.012-km² catchment (Figures 2 and 3c). Although this particular catchment did not burn in the Fish Fire, it is located within the SGM and was chosen for several reasons. First, the distribution of slope values within the catchment, referred to as Arroyo Seco, is similar to other debris-flow-producing basins in the SGM (Kean et al., 2011). Second, a terrestrial laser scanner survey of the entire Arroyo Seco site (Staley et al., 2014) provided a high-resolution digital elevation model (DEM) that could not be matched by any watershed at the Fish Fire site. Finally, the small size of the basin makes it

possible to perform the large number of simulations needed for hypothesis testing. We coarsened the DEM from its original resolution of 2 cm (Staley et al., 2014) to a grid spacing of 37.5 cm to further increase computational efficiency. Since the goal of this study is to understand debris-flow initiation thresholds and magnitude, as well as their sensitivity to rainfall characteristics and recovery, the location of the DEM relative to the perimeter of the Fish Fire is not critical; we focused on finding a DEM that is representative of the areas where post-fire debris flows tend to initiate in the SGM.

Runoff is driven by a set of idealized rainstorms (Figure 3b), with peak 15-minute rainfall intensities (I_{15}) varying from 10 to 60 mm/hr in increments of 5 mm/hr, as well as a family of rainstorms that are designed to have characteristics typical of an NCFR (Figures 2 and 3a). The storm events designed to represent an NCFR were generated through a two-step process. First, we identified a representative NCFR event impacting the SGM and extracted the rainfall data for that event. The selected event occurred on January 2, 2006, and had a well-defined narrow band of high intensity rainfall along the cold front.

Table 1. Model parameters used for simulations of runoff, sediment transport, and debris-flow initiation. Notation follows McGuire et al. (2016). When appropriate, values for years 1, 2, and 3 are presented and separated by commas. Median values are reported for K_s and h_f .

Parameter Name (Symbol)	Units	Value (Year 1, Year 2, Year 3)	Source
Roughness coefficient (n_0)	s/m ^{1/3}	0.05	Calibrated
Raindrop detachability (a_0)	kg/m/s	9,000	Calibrated
Raindrop redetachability (a_{d0})	kg/m/s	410,000	Calibrated
Fraction of effective stream power (F)	—	0.0065	Calibrated
Fraction canopy cover	—	0, 0.29, 0.77	Measured
Fraction bare soil	—	1, 0.63, 0.2	Measured
Field-saturated hydraulic conductivity (K_s)	mm/hr	19, 13, 28	Measured
Wetting front suction head (h_f)	m	0.006, 0.022, 0.026	Measured

It also exhibited the “gap and core” structure—cores of high-intensity precipitation separated by gaps of low-intensity precipitation—that is characteristic of an NCFR (e.g., Jorgensen et al., 2003) (Figure 2). Rainfall data from 18:16 and 19:46 UTC were extracted from the gauge at Clear Creek School (34°16′40, 118°10′15), which is maintained by the Los Angeles County Department of Public Works. The peak I_{15} of this storm is approximately 53 mm/hr (Figure 2). We then scaled the rainfall intensity of this NCFR by the amount needed in order to generate a series of NCFR-type rainstorms with peak values of I_{15} that match those of the family of idealized storms. The objective of this analysis is to take a first step toward exploring how different types of rainstorms may influence debris-flow response, even if their peak I_{15} is identical. The ratio of peak I_5 to peak I_{15} is a simple way to quantify a key difference between the family of idealized NCFRs and the family of designed rainstorms with a Gaussian distribution hyetograph, hereafter referred to simply as NCFRs and the designed rainstorms, respectively. The ratio I_5/I_{15} is approximately two to one for the NCFRs and one to four for the designed rainstorms.

All simulations were performed using the same parameters and model setup as reported in McGuire et al. (2017) unless otherwise noted (Table 1). Simulations begin with no runoff and an initial volumetric soil moisture content of 0.05. McGuire et al. (2016) calibrated the Hairsine-Rose sediment transport parameters at the Arroyo Seco site by comparing simulated erosion patterns to those generated from repeat terrestrial laser scanning surveys (Staley et al., 2014). The calibrated model was able to reproduce measured patterns of erosion and deposition as well as the timing of runoff and debris-flow activity at the outlet of the watershed during a monitored rainstorm in the first year following the Station Fire (McGuire et al., 2016, 2017). Here, the roughness coefficient is set to a value of $n_0 = 0.05$ s/m^{1/3}, which is in the range of calibrated roughness values for recently burned, low-order drainage basins in the SGM (Rengers et al., 2016a).

The fraction of bare soil exposed to raindrop impact is assumed to be 1.0 in the first year following the fire based on field observations of negligible vegetation and litter cover (Figure 2b). Infiltration rates were computed for year 1 using the K_s and h_f values obtained in September 2016 and November 2016, while K_s and h_f values obtained in July 2017 and March 2018 were used for year 2, and values measured in March 2019 were used for year 3 simulations. Each pixel within the computational domain was randomly assigned a value from the measured distribution of K_s and h_f . Due to the number of pixels in the computational domain, we found that differences among simulations performed with different realizations of K_s and h_f were not substantial. In locations where the slope exceeded 45°, we assumed that bedrock or saprolite was exposed at the surface and therefore set $K_s = 0$. A total of 7 out of 60 measurements attempted in September and November 2016 were terminated due to long measurement times (i.e., no measurable amount of water infiltrated within 5 minutes), potentially because of extreme water repellency or the presence of saprolite at very shallow depths. Including these data points in the analysis as locations with $K_s = 0$ and $h_f = 0$ did not significantly influence computed debris-flow thresholds or volumes, so they were neglected.

A total of 22 simulations were performed using the measured infiltration and vegetation characteristics from the first post-wildfire year. Eleven of these simulations were performed to assess how debris-flow properties change for the designed storms (Gaussian distribution of rainfall) with I_{15} varying from 10 to 60 mm/hr. Eleven additional simulations were used to assess how debris-flow properties change when using precipitation from an actual NCFR, with intensities scaled to give a different peak I_{15} varying from 10 to 60 mm/hr. A second and third set of numerical experiments, each containing 22 simulations, were performed using the measured infiltration and vegetation characteristics from the second and third post-wildfire years. Finally, we performed two final sets of simulations

Table 2. Summary of median and interquartile range (in parentheses) of soil-hydraulic properties as a function of time since burning.

Parameter Name (Symbol)	Units	Months						
		3 (n = 22)	5 (n = 31)	7 (n = 26)	8 (n = 37)	13 (n = 20)	21 (n = 21)	33 (n = 20)
Field-saturated hydraulic conductivity (K_s)	mm/hr	17 (18)	23 (23)	20 (30)	15 (18)	11 (21)	21 (32)	28 (37)
Sorptivity (S)	mm/hr ^{1/2}	3 (12)	11 (12)	11 (12)	7 (13)	18 (11)	20 (13)	25 (19)
Wetting front suction head (h_f)	m	0.002 (0.011)	0.008 (0.031)	0.016 (0.023)	0.004 (0.020)	0.032 (0.080)	0.021 (0.073)	0.026 (0.049)

using measured soil-hydraulic properties from year 2 and year 3 but vegetation characteristics (i.e., 100 percent bare ground) consistent with year 1. The goal of this last series of simulations was to quantify the relative impact of vegetation recovery and soil recovery on post-wildfire debris flows. Flow depth, discharge, and sediment concentration at the basin outlet were recorded in all cases to assess differences among simulations. Debris flows were identified at the outlet of the basin based on exceedance of a sediment concentration threshold of 40 percent. Flows with a sediment concentration (c) less than 40 percent were classified as floods. The amount of sediment exiting the basin (kg), sediment concentration (c) at the basin outlet, and peak debris-flow (i.e., flows with $c > 40$ percent) discharge at the outlet were stored for each simulation. Debris-flow volumes were estimated for each storm by determining the cumulative sediment discharge at the basin outlet during time periods when the sediment concentration exceeded 40 percent and then converting the resulting sediment mass to a volume by assuming a bulk density of 1,500 kg/m³. Summarizing debris flow size in terms of a volume allows for more direct comparisons with field-based estimates of debris-flow volume and outputs from empirical models used to predict debris-flow volume (e.g., Gartner et al., 2014).

RESULTS

Changes in Soil-Hydraulic Properties and Ground Cover

Repeat field measurements of soil-hydraulic properties reveal changes in sorptivity (S) and wetting front suction head (h_f) with time since burning. The median wetting front suction head (h_f) increased with time from roughly 0.002 m in September 2016 (3 months post-fire) to 0.026 m by March 2019 (33 months post-fire). A Kruskal-Wallis test indicates statistically significant differences among the seven different groups of h_f measurements ($p < 0.01$) made over the course of the 33-month monitoring period as well as differences among the seven groups of sorptivity measure-

ments ($p < 0.01$). Wilcoxon rank sum tests with a significance level of 0.05 were then used to assess differences between two groups of measurements to determine when significant changes occurred. According to a Wilcoxon rank sum test, the distributions of h_f after 3 and 5 months differ significantly ($p < 0.01$), as do the distributions of S after 3 and 5 months ($p < 0.01$). The distributions of h_f after 8 and 13 months also differ significantly ($p < 0.01$), as do the distributions of S after 8 and 13 months ($p < 0.01$). In addition to a change in the median of h_f between 8 and 13 months, there is also a substantial increase in the interquartile range from approximately 0.02 to 0.08 m (Table 2) that is consistent with a more general increase in the spread in the h_f distributions after 13 months of recovery (Figure 4). In contrast, field-saturated hydraulic conductivity (K_s) does not vary as systematically with time following the wildfire (Figure 4 and Table 2). A Kruskal-Wallis test indicates that measured distributions of K_s over the 33-month monitoring period ($p = 0.06$) are not significantly different. Despite a lack of statistical significance at the 0.05 level, both the mean and the median values of K_s increased substantially over the monitoring period. The median K_s increased from 17 mm/hr after 3 months to 28 mm/hr after 33 months, whereas the mean increased from 24 to 43 mm/hr over that same time period.

The fraction of bare soil decreased from 1.0 immediately following the wildfire to 0.63 in March 2018 after 21 months of recovery and 0.2 in March 2019 after 33 months of recovery. The reduction in bare ground was due primarily to an increase in canopy cover fraction from approximately 0 to 0.29 by March 2018 and 0.77 by March 2019. The fractions of litter cover were 0.07 and 0.03 in March 2018 and 2019, respectively, while rock cover was 0.01 and 0, respectively. Although the recovering vegetation may be effective at reducing direct raindrop impact on the soil surface, it likely had a minimal ability to intercept and store water, particularly in March 2018, since the average vegetation height was less than 10 cm. By March 2019, the mean canopy height had increased to approximately 80 cm.

Post-Fire Debris-Flow Initiation

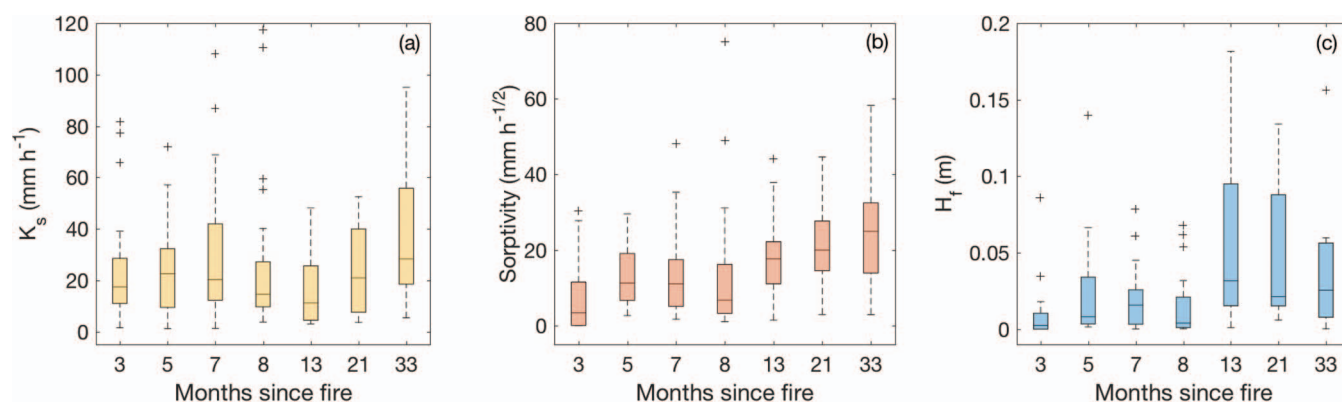


Figure 4. (a) Field-saturated hydraulic conductivity (K_s), (b) sorptivity (S), and (c) suction head (h_f) derived from field measurements at different times following the June 2016 Fish Fire.

Simulations of Erosion and Debris Flows

Debris flows initiated in response to lower-intensity rainstorms in year 1 relative to years 2 and 3 (Figure 5). The first sign of debris-flow activity at the lower outlet (i.e., debris-flow volume greater than 5 m^3) during year 1 occurs in response to the NCFR with a peak I_{15} of 15 mm/hr. In contrast, no debris flows initiate in response to the designed rainstorm (Gaussian distribution of rainfall) until the peak I_{15} is greater than or equal to 30 mm/hr. In year 2, simulations suggest that an NCFR with a peak I_{15} of at least 35 mm/hr is needed to produce a debris flow, whereas the peak I_{15} of the designed storm must exceed 40 mm/hr. In the theoretical case where vegetation recovery is neglected in year 2 and only changes in infiltration capacity are taken into account, the I_{15} required to produce a debris flow is 15 mm/hr for an NCFR and 35 mm/hr for the designed storm. In year 3, both the NCFR and the designed rainstorms having a peak I_{15} of 60 mm/hr failed to produce a debris flow with a volume greater than 5 m^3 (Figure 5). If vegetation recovery is neglected, then the I_{15} threshold for debris flows in year 3 would be 20 mm/hr for an NCFR and 50 mm/hr for the designed storm.

The volume of debris flows generated by NCFRs increases with peak I_{15} (Figure 5). The volume of debris flows initiated by the designed rainstorms tends to increase initially with I_{15} but then decreases slightly for higher values of I_{15} (Figure 5). The total volume of sediment eroded, however, continues to increase with peak I_{15} regardless of specifics of the hyetograph (Figure 5). Debris-flow volumes and total sediment eroded for a given rainstorm are highest in year 1, as expected. For a given I_{15} , the mean volume of debris flows generated by NCFRs in year 2 is, on average, less than one-third of that produced in year 1. The volume of debris flows generated by the designed storm in year

2 is, on average, roughly one-fourth of that generated in year 1. Changes in vegetation cover appear to play a key role in determining debris-flow volume. If vegetation recovery is negligible from year 1 to year 2, then mean debris-flow volumes associated with NCFRs and designed storms would differ by factors of only 1.2 and 1.1, respectively. It is also noteworthy that NCFRs tend to produce debris flows with greater peak discharges (Figure 5) and peak flow depths, as seen in the modeled hydrographs (Figure 6). NCFRs also produce debris flows that are larger than those produced by the designed storm, particularly when 15-minute rainfall intensities are above 50 mm/hr.

DISCUSSION

Field measurements constrain recovery timescales following disturbance by wildfire in the SGM (Figure 4 and Table 2) and provide insight into how soil and vegetation recovery translate into recovery from a debris-flow hazards perspective (Figures 5 and 6). Simulations of erosion and debris-flow initiation suggest that there should be a substantial increase in rainfall ID thresholds over the first 3 years of recovery following wildfire as well as decreases in expected debris-flow volume (Figure 5). Simulations do not take into account the reductions in sediment supply or increases in hydraulic roughness that are likely to occur due to sequential flow events between the first year and the third year after a wildfire (e.g., Tang et al., 2019). Results reported here can therefore be viewed as conservative, with even greater increases in ID thresholds and reductions in volume being likely in many natural systems.

Our field measurements indicate a significant change in the distributions of sorptivity (S) and suction head (h_f) between 3 and 5 months of recovery as well as between 8 and 13 months of recovery.

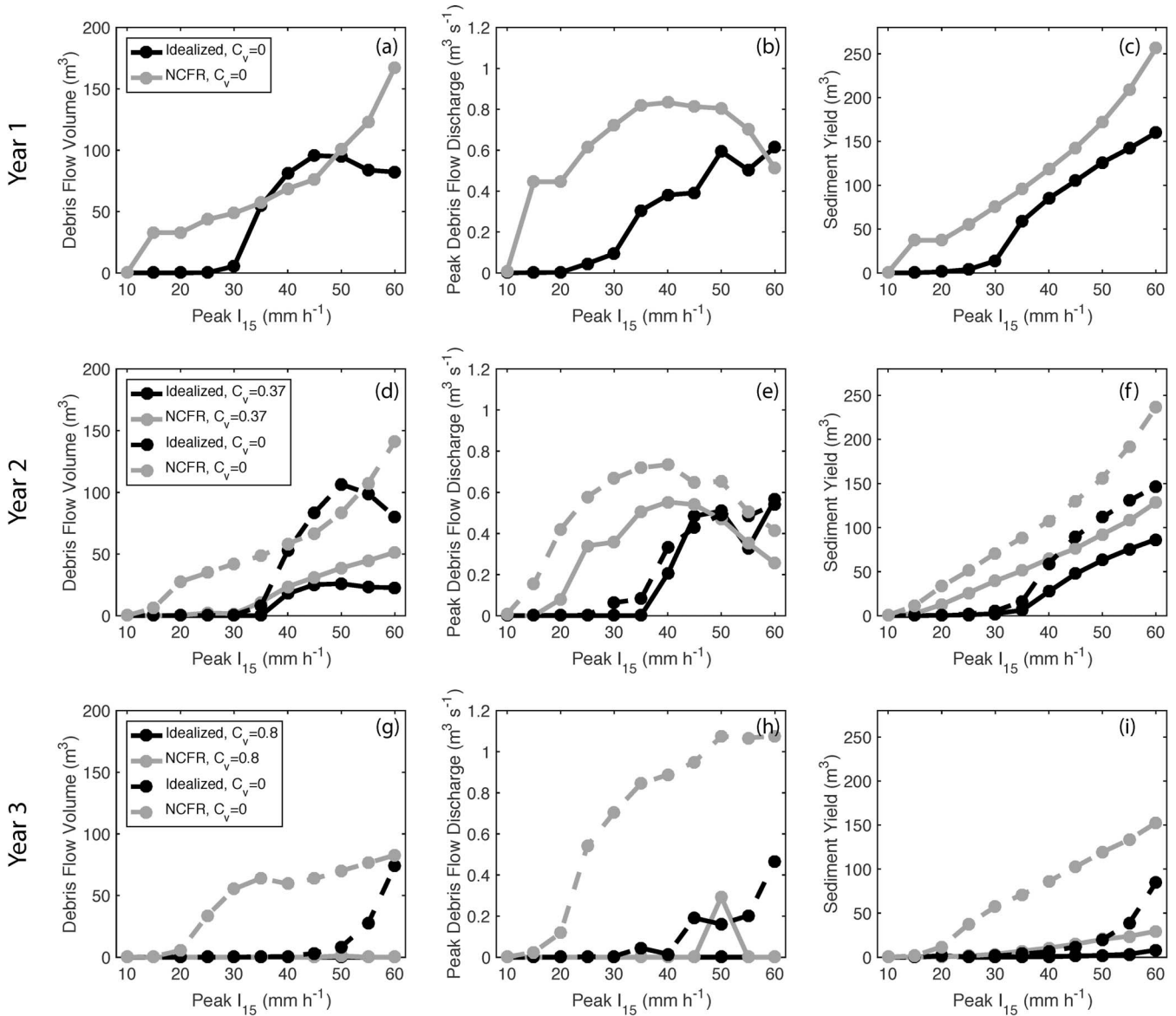


Figure 5. Model simulations of debris flow properties in (a–c) year 1, (d–f) year 2, and (g–i) year 3 in response to the two rainstorms with different peak values of I_{15} . The combined fraction of vegetation and ground cover is denoted by C_v .

However, it is not clear whether the change in S and h_f between 3 and 5 months was due to recovery or due to the change in measurement location that took place between 3 and 5 months. Low values of S and h_f in the year immediately following wildfire are consistent with a recent compilation of soil-hydraulic properties from burned soils (Ebel and Moody, 2017). Previous studies monitoring temporal changes in soil-hydraulic properties after fire have often focused more on quantifying field-saturated hydraulic conductivity (K_s). Cerdá (1998), for example, used rainfall simulation experiments to measure a doubling of K_s from 25 mm/hr after 7 months of recovery following a fire in a Mediterranean scrubland to 52 mm/hr following 64

months of recovery. Robichaud et al. (2016) also report a substantial increase in K_s from 31 mm/hr within 1 month of the Valley Complex fire to 38 mm/hr after 11 months and 84 mm/hr after 60 months. Using a Kruskal-Wallis test and a significance level of 0.05, we find no statistically significant changes in the distribution of K_s with time following the Fish Fire. Still, the median and mean values of K_s were substantially greater 33 months after the fire relative to 3 months after the fire. Combined with increases in S over that same time period, potentially large implications for runoff generation may be underestimated by examining differences in S and K_s individually. Improved understanding of the timescales over which soil-hydraulic

Post-Fire Debris-Flow Initiation

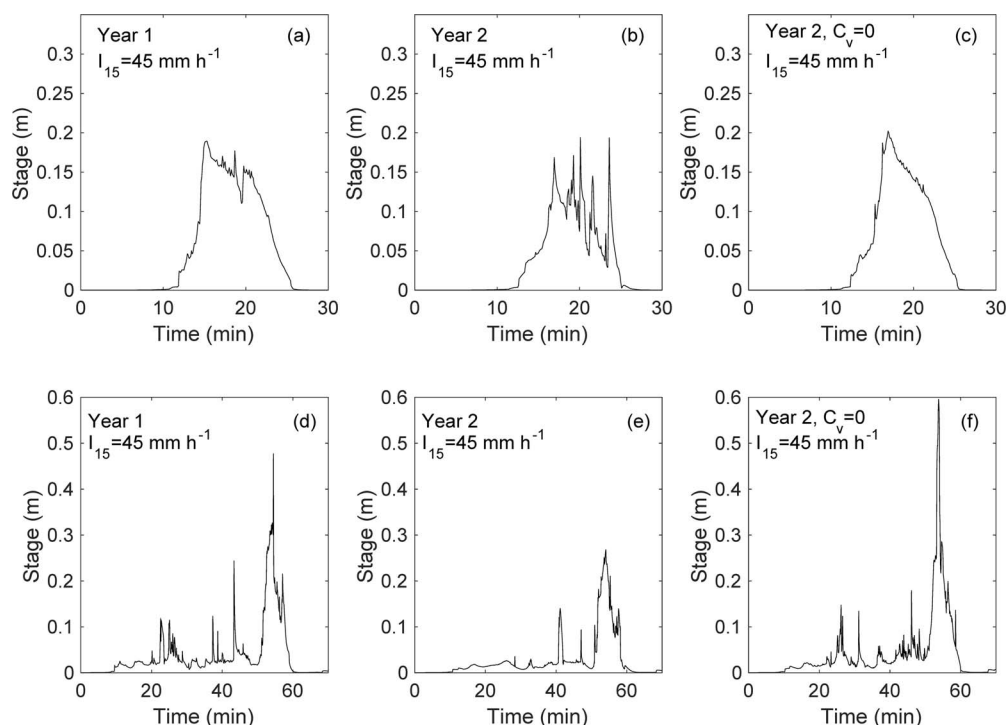


Figure 6. Model simulations of flow stage at the Arroyo Seco basin outlet in response to (a–c) the designed storm with peak $I_{15} = 45$ mm/hr and (d–f) a narrow cold-frontal rain band with peak $I_{15} = 45$ mm/hr under different conditions.

properties recover following fire are crucial for quantifying when recently burned landscapes will regain hydrologic function (e.g., Ebel and Mirus, 2014), including when debris-flow potential will return to that of long-unburned areas.

Measurements of soil-hydraulic properties and vegetation/ground cover can be used in conjunction with the numerical model to infer year 1 debris-flow thresholds of $I_{15} = 15$ mm/hr and $I_{15} = 30$ mm/hr for an NCFR and the designed storm, respectively (Figure 5). The regional I_{15} threshold of 19 mm/hr for debris flow initiation in the SGM (Staley et al., 2013) falls in between these two model-derived thresholds. We attribute the lower I_{15} threshold for NCFRs to greater rainfall intensities over shorter durations, as quantified by the relatively high I_5/I_{15} ratio relative to the designed storm, which was more effective at generating runoff. It is also possible that thresholds associated with NCFRs are lower due to the presence of roughly 50 minutes of low-intensity rainfall that precedes the peak (Figure 2). However, this is unlikely to be a dominant factor in post-fire year 1, when the differences in debris-flow thresholds between the two rainstorms are most accentuated. First, the modeled I_{15} threshold associated with NCFRs in year 1 is 15 mm/hr. The average rainfall intensity during the first 45 minutes of that storm is approximately 7 mm/hr, which is not sufficient to generate runoff or trans-

port sediment, and the total depth of rainfall during that time period would be less than 6 mm. Even if the first 45 minutes of rainfall were eliminated from all NCFRs, the I_{15} threshold in year 1 would increase from only 15 to 20 mm/hr. The observation that NCFRs tend to produce debris flows at a lower I_{15} relative to the designed storm suggests that particular attention should be given to debris-flow potential when atmospheric conditions are conducive to producing an NCFR. Further work is needed to quantify the ability of NCFRs to produce debris flows relative to other types of storm systems known to produce intense rainfall in southern California, such as isolated convective cells.

Increases in the I_{15} threshold associated with NCFRs from 15 mm/hr in year 1 to 35 mm/hr in year 2 can be attributed primarily to decreases in the percentage of bare ground. We documented an increase in the wetting front suction head (h_f) from year 1 to year 2 (Table 1 and Figure 4), but the I_{15} threshold would still remain constant at 15 mm/hr in years 1 and 2 if vegetation recovery were completed neglected (Figure 5). The ID threshold associated with the designed storm, on the other hand, increased from 30 mm/hr in year 1 to 40 mm/hr in year 2 (Figure 5). Since the threshold would be 35 mm/hr in the case where vegetation recovery is neglected in year 2, approximately half of the increase from 30 to 40 mm/hr can be

attributed to vegetation recovery. The remainder of the increase can be related to changes in soil-hydraulic properties, namely, the increase in h_f that took place between 8 and 13 months after the wildfire. All else being equal, lower values of h_f will lead to an increase in runoff. Decreases in percent bare ground will lead to less hillslope erosion, which subsequently decreases the amount of sediment transported into the channel network (where debris flows are likely to form) and reduces the sediment-bulking processes that can increase flow depths and discharges. Simulations suggest that the ability of NCFRs to produce debris flows is particularly sensitive to changes in vegetation/ground cover. Therefore, the initiation of debris flows via NCFRs at our study site appears to be more sensitive to changes in the efficiency of hillslope erosion relative to the designed storms.

Simulations also offer insight into how debris-flow magnitude can be expected to change with rainfall intensity and time since burning for the two different storms. Simulations indicate that debris-flow volume generally increases monotonically with I_{15} for NCFRs (Figure 5). This is consistent with Gartner et al. (2014), who found that debris-flow volumes increase with I_{15} based on a large data set of estimated volumes from post-wildfire debris flows throughout the Transverse Ranges of southern California. In contrast, debris-flow volume mobilized by the designed storms does decrease slightly when I_{15} is greater than 45 mm/hr in years 1 and 2. The difference between our model results and field observations (e.g., Gartner et al., 2014) could be due partly to the definition of debris flow employed here, which requires that the sediment concentration exceed 40 percent. In some of the model scenarios, an increase in I_{15} leads to more runoff and an overall reduction in sediment concentration to values less than 40 percent. Since debris-flow volumes estimated in the field are based on the amount of sediment deposited in debris basins or estimates of erosion occurring during debris-flow-producing rainstorms (e.g., Gartner et al., 2014), they may include sediment transported through a combination of water-dominated flood, debris flood, and debris-flow mechanisms. Regardless, debris flows with the greatest volume, highest peak discharge, and largest flow depths are generally produced by NCFRs with high rainfall intensities (Figures 5 and 6). Simulations also indicate a rapid decrease in expected debris-flow volume between post-fire years 1 and 2. Santi and Morandi (2013) analyzed post-wildfire debris-flow volumes from California and also found a substantial decrease in volume between debris flows generated within 1 year of a fire and those generated between 1 and 3 years after fire, with the median sediment yield from debris flows decreasing from 10,156 to 4,006 m^3/km^2 .

While we focus on a particular geographic region, the SGM in southern California, the modeling framework presented here can be used in combination with estimates of post-wildfire infiltration rates from other regions (e.g., Moody et al., 2009; Nyman et al., 2011; and Robichaud et al., 2016) to quantify the impact of changing soil-hydraulic properties on debris-flow magnitude and initiation thresholds. Similarly, satellite-derived metrics of vegetation recovery, such as the enhanced vegetation index (e.g., Kinoshita and Hogue, 2011), could be used to drive temporal changes in percent ground cover within the model framework. Developing relationships between measurable hydrologic variables, ground cover characteristics, and debris-flow properties is a necessary first step toward assessing how debris-flow threats are likely to evolve with time following wildfire in different geographic regions. The prevalence of NCFRs as a primary driver of high-intensity precipitation is also somewhat specific to this region, but the results here suggest that the temporal distribution of rainfall within a storm can impact rainfall thresholds for runoff-generated debris flows. Here, we explore differences between only one storm type (NCFRs) and its associated hyetograph and a Gaussian distribution of rainfall. Additional work is needed to determine the difference in debris-flow characteristics across other storm types (and their associated hyetographs) that regularly impact the Transverse Ranges.

One key benefit of assessing how debris-flow response varies as a function of storm type (e.g., NCFR versus a designed storm), is that it has the potential to increase the situational awareness of weather forecasters concerned with debris-flow hazards. Precipitation forecasts become more uncertain as lead time increases (e.g., Wick et al., 2013), and it is difficult to accurately forecast the location, timing, and intensity of short-duration, high-intensity rainfall (Doswell et al., 1996) at lead times that are useful to emergency management (at least 24–36 hours). However, forecasters can look for the presence or absence of a certain set of atmospheric conditions that they may associate with the potential for a particular type of high-intensity rainfall event (e.g., an NCFR). If the forecaster is aware of the debris-flow response associated with the typical hyetograph of that characteristic storm type, this would provide them with additional confidence about the potential for an impactful debris flow in the area of concern.

CONCLUSIONS

Disturbance following wildfire leads to an increased potential for runoff-generated debris flows. The hazards posed by runoff-generated debris flows decrease

with time following wildfire as soil and vegetation recover. In this study, we monitored changes in soil-hydraulic properties and percent bare ground at a site in southern California and used a numerical model to determine how temporal changes in these two variables affect debris-flow volumes and initiation thresholds. The fraction of bare ground at our study area decreased from approximately 1.0 immediately following the fire to 0.63 after 21 months and to 0.2 after 33 months. Both sorptivity and wetting front suction head increased significantly after 13 months of recovery and generally increased with time following the wildfire. Simulations suggest that the threshold I_{15} rainfall intensity that triggers debris flows at our study site in the SGM is sensitive to how rainfall is distributed in time. The I_{15} threshold for an NCFR could be as low as 15 mm/hr in post-fire year 1 and 35 mm/hr in year 2. A designed rainstorm with a time series of rainfall distributed like a Gaussian function was responsible for producing debris flows only when I_{15} was greater than 30 mm/hr in year 1 and 40 mm/hr in year 2. Regardless of the temporal distribution of rainfall within a storm, if debris flows do initiate in the second post-wildfire year, simulations indicate that they will be roughly one-third to one-fourth the volume of those generated in year 1. Results demonstrate how debris-flow thresholds and magnitude can be sensitive to the time series of rainfall and identify the need to quantify how/why different types of storms may be more or less likely to produce impactful debris flows. Although we focus here on post-wildfire debris flows, the methodology used to assess changes in runoff-generated debris-flow susceptibility could be applied in other settings, including rocky alpine regions, where runoff-generated debris flows may occur.

ACKNOWLEDGMENTS

This work was supported in part by the National Oceanic and Atmospheric Administration (NOAA) Collaborative Science, Technology, and Applied Research (CSTAR) Program under grant NA19NWS4680004 and by the U.S. Geological Survey (USGS) Landslide Hazards Program. Any use of trade, product, or firm names is for descriptive purposes only and does not imply endorsement by the U.S. government. Code for the numerical model used in this study (SWEHR) is available through the Community Surface Dynamics Modeling System (CSDMS) model repository.

REFERENCES

- CANNON, S. H.; GARTNER, J. E.; WILSON, R. C.; BOWERS, J. C.; AND LABER, J. L., 2008, Storm rainfall conditions for floods and debris flows from recently burned areas in southwestern Colorado and southern California: *Geomorphology*, Vol. 96, No. 3–4, pp. 250–269.
- CANNON, S. H.; KIRKHAM, R. M.; AND PARISE, M., 2001, Wildfire-related debris flow initiation processes, Storm King Mountain, Colorado: *Geomorphology*, Vol. 39, pp. 171–188.
- CERDÁ, A., 1998, Changes in overland flow and infiltration after a rangeland fire in a Mediterranean scrubland: *Hydrological Processes*, Vol. 12, pp. 1031–1042.
- CROCKER, R. L. AND TIVER, N. S., 1948, Survey methods in grassland ecology: *Grass and Forage Science*, Vol. 3, No. 1, pp. 1–26.
- DEBANO, L. F., 2000, The role of fire and soil heating on water repellency in wildland environments: A review: *Journal of Hydrology*, Vol. 231, pp. 195–206.
- DOSWELL, C.A. III; BROOKS, H. E.; AND MADDOX, R. A., 1996, Flash flood forecasting: An ingredients-based methodology: *Weather and Forecasting*, Vol. 11, No. 4, pp. 560–581.
- EBEL, B. A. AND MIRUS, B. B., 2014, Disturbance hydrology: Challenges and opportunities: *Hydrological Processes*, Vol. 28, No. 19, pp. 5140–5148.
- EBEL, B. A. AND MOODY, J. A., 2017, Synthesis of soil-hydraulic properties and infiltration timescales in wildfire-affected soils: *Hydrological Processes*, Vol. 31, No. 2, pp. 324–340.
- GABET, E. J. AND BOOKER, A., 2008, A morphometric analysis of gullies scoured by post-fire progressively bulked debris flows in southwest Montana, USA: *Geomorphology*, Vol. 96, No. 3–4, pp. 298–309.
- GARTNER, J. E.; CANNON, S. H.; AND SANTI, P. M., 2014, Empirical models for predicting volumes of sediment deposited by debris flows and sediment-laden floods in the transverse ranges of southern California: *Engineering Geology*, Vol. 176, pp. 45–56.
- HAIRSINE, P. B. AND ROSE, C. W., 1992a, Modeling water erosion due to overland flow using physical principles: 1. Sheet flow: *Water Resources Research*, Vol. 28, No. 1, pp. 237–243.
- HAIRSINE, P. B. AND ROSE, C. W., 1992b, Modeling water erosion due to overland flow using physical principles: 2. Rill flow: *Water Resources Research*, Vol. 28, No. 1, pp. 245–250.
- IVERSON, R. M. AND DENLINGER, R. P., 2001, Flow of variably fluidized granular masses across three-dimensional terrain: 1. Coulomb mixture theory: *Journal of Geophysical Research: Solid Earth*, Vol. 106, No. B1, pp. 537–552.
- JORGENSEN, D. P.; PU, Z.; PERSSON, P. O.; AND TAO, W., 2003, Variations associated with cores and gaps of a Pacific narrow cold frontal rainband: *Monthly Weather Review*, Vol. 131, pp. 2705–2729.
- KEAN, J. W.; MCCOY, S. W.; TUCKER, G. E.; STALEY, D. M.; AND COE, J. A., 2013, Runoff-generated debris flows: Observations and modeling of surge initiation, magnitude, and frequency: *Journal of Geophysical Research: Earth Surface*, Vol. 118, No. 4, pp. 2190–2207.
- KEAN, J. W.; STALEY, D. M.; AND CANNON, S. H., 2011, In situ measurements of post-fire debris flows in southern California: Comparisons of the timing and magnitude of 24 debris-flow events with rainfall and soil moisture conditions: *Journal of Geophysical Research*, Vol. 116, F04019. doi:10.1029/2011JF002005.
- KEAN, J. W.; STALEY, D. M.; LANCASTER, J. T.; RENGERS, F. K.; SWANSON, B. J.; COE, J. A.; HERNANDEZ, J. L.; SIGMAN, A. J.; ALLSTADT, K. E.; AND LINDSAY, D. N., 2019, Inundation, flow dynamics, and damage in the 9 January 2018 Montecito debris-flow event, California, USA: Opportunities and challenges for post-wildfire risk assessment: *Geosphere*, Vol. 15, No. 4, pp. 1140–1163.

- KINOSHITA, A. M. AND HOGUE, T. S., 2011, Spatial and temporal controls on post-fire hydrologic recovery in Southern California watersheds: *Catena*, Vol. 87, No. 2, pp. 240–252.
- LARSEN, I. J.; MACDONALD, L. H.; BROWN, E.; ROUGH, D.; WELSH, M. J.; PIETRASZEK, J. H.; LIBOHOVA, Z.; DE DIOS BENAVIDES-SOLORIO, J.; AND SCHAFFRATH, K., 2009, Causes of post-fire runoff and erosion: Water repellency, cover, or soil sealing?: *Soil Science Society of America Journal*, Vol. 73, No. 4, pp. 1393–1407.
- MCGUIRE, L. A.; KEAN, J. W.; STALEY, D. M.; RENGERS, F. K.; AND WASKLEWICZ, T. A., 2016, Constraining the relative importance of raindrop- and flow-driven sediment transport mechanisms in post-wildfire environments and implications for recovery time scales: *Journal of Geophysical Research: Earth Surface*. doi:10.1002/2016JF003867.
- MCGUIRE, L. A.; RENGERS, F. K.; KEAN, J. W.; AND STALEY, D. M., 2017, Debris flow initiation by runoff in a recently burned basin: Is grain-by-grain sediment bulking or en masse failure to blame?: *Geophysical Research Letters*, Vol. 44, No. 14, pp. 7310–7319.
- MEYER, G. A. AND WELLS, S. G., 1997, Fire-related sedimentation events on alluvial fans, Yellowstone National Park, USA: *Journal of Sedimentary Research*, Vol. 67, No. 5, pp. 776–791.
- MOODY, J. A. AND EBEL, B. A., 2012, Hyper-dry conditions provide new insights into the cause of extreme floods after wildfire: *Catena*, Vol. 93, pp. 58–63.
- MOODY, J. A.; KINNER, D. A.; AND ÚBEDA, X., 2009, Linking hydraulic properties of fire-affected soils to infiltration and water repellency: *Journal of Hydrology*, Vol. 379, No. 3–4, pp. 291–303.
- MOODY, J. A.; SMITH, J. D.; AND RAGAN, B. W., 2005, Critical shear stress for erosion of cohesive soils subjected to temperatures typical of wildfires: *Journal of Geophysical Research: Earth Surface*, Vol. 110, No. F01004. doi:10.1029/2004JF000141.
- MÜGLER, C.; PLANCHON, O.; PATIN, J.; WEILL, S.; SILVERA, N.; RICHARD, P.; AND MOUCHE, E., 2011, Comparison of roughness models to simulate overland flow and tracer transport experiments under simulated rainfall at plot scale: *Journal of Hydrology*, Vol. 402, No. 1–2, pp. 25–40.
- NYMAN, P.; SHERIDAN, G. J.; SMITH, H. G.; AND LANE, P. N., 2011, Evidence of debris flow occurrence after wildfire in upland catchments of south-east Australia: *Geomorphology*, Vol. 125, No. 3, pp. 383–401.
- OAKLEY, N. S.; CANNON, F.; MUNROE, R.; LANCASTER, J. T.; GOMBERG, D.; AND RALPH, F. M., 2018, Brief communication: Meteorological and climatological conditions associated with the 9 January 2018 post-fire debris flows in Montecito and Carpinteria California, USA: *Natural Hazards and Earth System Sciences*, Vol. 18, pp. 3037–3043.
- OAKLEY, N. S.; LANCASTER, J. T.; KAPLAN, M. L.; AND RALPH, F. M., 2017, Synoptic conditions associated with cool season post-fire debris flows in the Transverse Ranges of southern California: *Natural Hazards*, Vol. 88, pp. 327–354.
- PARSON, A.; ROBICHAUD, P. R.; LEWIS, S. A.; NAPPER, C.; AND CLARK, J. T., 2010, *Field Guide for Mapping Post-Fire Soil Burn Severity: U.S. Department of Agriculture Forest Service General Technical Report RMRS-GTR-243*, 49 p.
- RAYMOND, C. A.; MCGUIRE, L. A.; YOUNBERG, A. M.; STALEY, D. M.; AND KEAN, J. W., 2020, Thresholds for post-wildfire debris flows: Insights from the Pinal Fire, Arizona, USA: *Earth Surface Processes and Landforms*, Vol. 45, No. 6, pp. 1349–1360.
- RENGERS, F. K.; MCGUIRE, L. A.; KEAN, J. W.; STALEY, D. M.; AND HOBLEY, D., 2016a, Model simulations of flood and debris flow timing in steep catchments after wildfire: *Water Resources Research*, Vol. 52, pp. 6041–6061.
- RENGERS, F. K.; TUCKER, G. E.; MOODY, J. A.; AND EBEL, B. A., 2016b, Illuminating wildfire erosion and deposition patterns with repeat terrestrial lidar: *Journal of Geophysical Research: Earth Surface*, Vol. 121, No. 3, pp. 588–608.
- ROBICHAUD, P. R.; WAGENBRENNER, J. W.; PIERSON, F. B.; SPAETH, K. E.; ASHMUN, L. E.; AND MOFFET, C. A., 2016, Infiltration and interrill erosion rates after a wildfire in western Montana, USA: *Catena*, Vol. 142, pp. 77–88.
- SANTI, P. M. AND MORANDI, L., 2013, Comparison of debris-flow volumes from burned and unburned areas: *Landslides*, Vol. 10, No. 6, pp. 757–769.
- SHAKESBY, R. A. AND DOERR, S. H., 2006, Wildfire as a hydrological and geomorphological agent: *Earth-Science Reviews*, Vol. 74, No. 3–4, pp. 269–307.
- SMITH, H. G.; SHERIDAN, G. J.; NYMAN, P.; CHILD, D. P.; LANE, P. N.; HOTCHKIS, M. A.; AND JACOBSEN, G. E., 2012, Quantifying sources of fine sediment supplied to post-fire debris flows using fallout radionuclide tracers: *Geomorphology*, Vol. 139, pp. 403–415.
- STALEY, D. M.; KEAN, J. W.; CANNON, S. H.; LABER, J. L.; AND SCHMIDT, K. M., 2013, Objective definition of rainfall intensity-duration thresholds for the initiation of post-fire debris flows in southern California: *Landslides*, Vol. 10, pp. 547–562.
- STALEY, D. M.; NEGRI, J. A.; KEAN, J. W.; LABER, J. L.; TILLERY, A. C.; AND YOUNBERG, A. M., 2017, Prediction of spatially explicit rainfall intensity-duration thresholds for post-fire debris-flow generation in the western United States: *Geomorphology*, Vol. 278, pp. 149–162.
- STALEY, D. M.; WASKLEWICZ, T. A.; AND KEAN, J. W., 2014, Characterizing the primary material sources and dominant erosional processes for post-fire debris-flow initiation in a headwater basin using multi-temporal terrestrial laser scanning data: *Geomorphology*, Vol. 214, pp. 324–338.
- STOOF, C. R.; VERVOORT, R. W.; IWEMA, J.; ELSSEN, E.; FERREIRA, A. J. D.; AND RITSEMA, C. J., 2012, Hydrological response of a small catchment burned by experimental fire: *Hydrology and Earth System Sciences*, Vol. 16, No. 2, pp. 267–285.
- TAKAHASHI, T., 1978, Mechanical characteristics of debris flow: *Journal of the Hydraulics Division of the American Society of Civil Engineers*, Vol. 104, No. 8, pp. 1153–1169.
- TANG, H.; MCGUIRE, L. A.; RENGERS, F. K.; KEAN, J. W.; STALEY, D. M.; AND SMITH, J. B., 2019, Evolution of debris-flow initiation mechanisms and sediment sources during a sequence of post wildfire rainstorms: *Journal of Geophysical Research: Earth Surface*, Vol. 124, pp. 1572–1595.
- VANDERVAERE, J. P.; VAUCLIN, M.; AND ELRICK, D. E., 2000, Transient flow from tension infiltrometers II. Four methods to determine sorptivity and conductivity: *Soil Science Society of America Journal*, Vol. 64, pp. 1272–1284.
- WICK, G. A.; NEIMAN, P. J.; RALPH, F. M.; AND HAMILL, T. M., 2013, Evaluation of forecasts of the water vapor signature of atmospheric rivers in operational numerical weather prediction models: *Weather and Forecasting*, Vol. 28, No. 6, pp. 1337–1352.
- ZHANG, R., 1997, Determination of soil sorptivity and hydraulic conductivity from the disk infiltrometer: *Soil Science Society of America Journal*, Vol. 61, No. 4, pp. 1024–1030.